




Coverage of a shopping mall with flexible OLED-based visible light communications

ZAHRA NAZARI CHALESHTORI,^{1,*} STANISLAV ZVANOVEC,¹ ZABIH GHASSEMLOOY,²  HOSSIEEN B. ELDEEB,³ AND MURAT UYSAL³

¹Department of Electromagnetic Field, Faculty of Electrical Engineering, Czech Technical University in Prague, Prague 16627, Czech Republic

²Optical Communications Research Group, Faculty of Engineering and Environment, Northumbria University, Newcastle-upon-Tyne NE1 8ST, UK

³Department of Electrical and Electronics Engineering, Ozyegin University, Istanbul 34794, Turkey
[*nazarzah@fel.cvut.cz](mailto:nazarzah@fel.cvut.cz)

Abstract: Visible light communications (VLC) can utilize light-emitting diodes (LEDs) to provide illumination and a safe and low-cost broadcasting network simultaneously. In the past decade, there has been a growing interest in using organic LEDs (OLEDs) for soft lighting and display applications in public places. Organic electronics can be mechanically flexible, thus the potential of curved OLED panels/displays devices. This paper provides unique characteristics of a flexible OLED-based VLC link in a shopping mall. We show that, for curved OLED the radiation pattern displays a symmetry, which is wider than Lambertian. A number of scenarios of VLC system with flexible OLED are analyzed. Numerical models for the delay spread and optical path loss are derived, which followed a 2-term power series model for both empty and furnished rooms. We show that using a full-circular OLED for both empty and furnished rooms offers a uniform distribution of emitted power for the same transmission link spans. The link performance using full and half-circular OLED in an empty room shows that the average optical path losses are lower by 5 and 4 dB, compared with the furnished room.

© 2020 Optical Society of America under the terms of the [OSA Open Access Publishing Agreement](#)

1. Introduction

Visible light communications (VLC) provide illumination and wireless data transmission through the free space at the same time via intensity modulation of the light source [1,2]. In VLC, both the conventional silicon-based light-emitting diodes (LEDs) and organic-based LEDs (OLEDs), which are widely used as lamps and panels in homes, public places and offices, can be adopted [3,4]. In this work, we only consider OLEDs, where the emissive electroluminescent layer is a film of organic compounds, are thinner, lighter and more flexible than the crystalline layers in LEDs or liquid crystal display (LCD) devices [5]. With improved technologies and reduced fabrication and manufacturing costs, OLEDs offer an advantage over the conventional LEDs and other lighting technologies including self-emission, brighter with rich colors, biodegradable, wide beam angle, simple and flexible structure, with no need for backlighting and large active areas [6,7]. However, OLEDs are costly to produce with shorter lifetimes (in particular blue organics) and can be damaged by water. In addition, OLEDs have a low modulation bandwidth B_{mod} of hundreds of kHz compared with solid-state LEDs (a few MHz), which are due to the carrier lifetime and the parasitic resistor-capacitor (RC) effects [8]. An exciting feature of OLED panels is the potential of using flexible substrates to make lights that can be curved, rolled or folded.

Note, in VLC wavelength-dependence channel modeling, it is important to consider the reflectance properties of the materials and objects within the indoor environments. To determine channel impulse response (CIR) of VLC systems, a number of research activities have been reported, which emphasize the use of inorganic LEDs. For instance, in [9], to find CIR of the

VLC system in an empty room, Monte Carlo ray-tracing method was adopted considering up to 3 reflections. However, the majority of published works do not consider the wavelength dependency of the channel. Works in [10,11] used recursive calculation methods [12] to determine CIR of an empty room without considering wavelength dependency. In [13], Barry's model by including wavelength-dependent white LED characteristics and spectral reflectance of indoor reflectors was generalized and up to 4 reflections are considered to model indoor multipath dispersion characteristics for VLC. Next, in [14], Barry's model was compared with channel modeling results obtained using a commercial optical and illumination design software Zemax [15] and the approach yielded the same CIR as in [13]. In this approach, a larger number of reflections and the wavelength-dependency of the materials can be included and it has been endorsed as a reference channel model for upcoming standards such as IEEE 802.15.7r1 [16]. In [17], for VLC a three-dimensional (3D) simulation environment using a CAD software was model based on Monte Carlo algorithm. In [18], flexible OLED lighting panel radiation pattern and its impact on the VLC channel were investigated. It was shown that, compared with Lambertian source, OLEDs are more flexible in terms of the radiation pattern control offering reduced root mean square (RMS) delay spread and the average optical path loss (OPL) of 8.8% and 3 dB, respectively.

The use of curved OLED with a wider beam pattern than Lambertian for VLC for different indoor scenarios has not been reported in the literature yet. Additionally, as the development of organic technology is being increased at applications of large display panels and pixels used in mobile devices, there is a significant potential to facilitate simultaneously illumination, display with text message on it, and data communication via the display of screens provided in shopping malls. In this paper, a flexible OLED used in a shopping mall is investigated by the means of characterizing its illumination profile, spectrum and B_{mod} . For simulating the channel-specific features, we have adopted ray tracing. The specific channel models in terms of OPL and RMS delay spread are derived for four scenarios within the shopping mall. A full and half-circular OLED are placed around the pillar in an empty and a furnished room with different size of a transmitter (Tx) and varied locations of a receiver (Rx). In addition, the performance of an OLED-based VLC link is investigated in terms of the bit error rate (BER). Using full and half-circular OLEDs in an empty room, data rates R_b of 10 Mb/s and 3.7 Mb/s are achieved over a line of sight (LOS) path of 6 m, respectively. The data rate is dropped to 1.02 Mb/s and 0.46 Mb/s in a furnished room, respectively.

The rest of the paper is organized as follows. In Section 2, the principle of the VLC channel and OLED specifics are described. Section 3 represents the main features of the simulation and Section 4 discusses the results. Finally, conclusions are given in Section 5.

2. Principle of VLC

2.1. Channel characterization

The physical indoor VLC channel includes the effects of both LOS, where the LED is aligned directly with the Rx, and non-LOS (NLOS), where the signal is captured via reflections from walls, ceiling, etc., [19]. The regenerated electrical signal at the output of the optical Rx is given as [1]:

$$y(t) = \gamma \cdot x(t) \otimes h(t) + n(t), \quad (1)$$

where $x(t)$ is the emitted optical intensity, γ is the photodetector (PD) responsivity in (A/W), $h(t)$ is the CIR and \otimes denotes convolution. $n(t)$ represents the noise, which includes the quantum noise from the optical signal, background radiation noise caused by the photons reception from ambient light and noise from the Rx such as the dark current noise and the thermal noise. The background radiation noise can be modeled as the signal independent additive white Gaussian noise (AWGN) with one-sided power spectral density N_0 due to its high intensity. The background radiation

induced noise limits the received signal-to-noise ratio (SNR) since it is the dominant noise source [20]. The CIR of the indoor channel can be written as $\sum_{i=1}^N \eta_i \delta(t - \tau_i)$, where $\delta(t)$ is Dirac delta function, τ_i is the time delay of the i^{th} ray, η_i is the gain path of the i^{th} ray and N is the number of received rays [1]. We consider three criteria to quantify the limitation on the transmission rate through the free space channel; channel gain and corresponding OPL = $-10 \log_{10} (\int_{-\infty}^{\infty} h(t) dt)$ in dB, channel mean excess delay τ and the RMS delay spread τ_{RMS} , which are given as [14]:

$$\tau = \frac{\int_0^{\infty} t \times h(t) dt}{\int_0^{\infty} h(t) dt}, \quad (2)$$

$$\tau_{RMS} = \sqrt{\frac{\int_0^{\infty} (t - \tau)^2 \times h(t) dt}{\int_0^{\infty} h(t) dt}}. \quad (3)$$

The optical radiation pattern profile determines the spatial intensity distribution of light emitted from the light source. The luminous intensity defined in terms of the angle of irradiance θ is given as [1]:

$$I(\theta) = \frac{m_L + 1}{2\pi} I(0) \cos^{m_L}(\theta) \quad \theta = \left[-\frac{\pi}{2}, \frac{\pi}{2} \right], \quad (4)$$

where $I(0)$ is the center luminous intensity of the LED and m_L is Lambertian order, which is defined in terms of the Tx semi-angle $\theta_{1/2}$ as [1]:

$$m_L = -\frac{\ln(2)}{\ln[\cos(\theta_{1/2})]}. \quad (5)$$

2.2. OLEDs

2.2.1. Structure of OLEDs

OLED display devices use organic carbon-based films, sandwiched together between two charged electrodes; one is a metallic cathode (aluminum or silver) and the other is a transparent anode (indium tin oxide (ITO)), see Fig. 1 [21]. The organic materials can be long-chain polymers (i.e., PLEDs) or small organic molecules (i.e., SMOLEDs) in a crystalline phase. Note, OLEDs have a low-pass filter transfer function with the cut-off frequency given by [1]:

$$f_c = \frac{1}{2\pi RC_o}, \quad (6)$$

where R is the effective resistance of the OLED and $C_o = \frac{A_t \epsilon_0 \epsilon_r}{d}$ is the plate capacitance, A_t is the OLED photoactive area, d is the OLED thickness, and ϵ_0 and ϵ_r are the permittivities of free space and relative dielectric constant of the organic layer, respectively. Evidently, a larger area photoactive will have a lower B_{mod} and hence a limitation on the maximum R_b in OVLC systems. Flexibility and lower production cost of non-rigid OLEDs make them the light source for future applications. The curved or rolled OLED panels/displays can be used in wearable products (such as wearable smart watches and computers), mobile phones, TVs, vehicles, trains, etc.

2.2.2. Characterization of a flexible OLED

A flexible OLED (UNISAGA, the size of $200 \times 50 \text{ mm}^2$) was characterized in terms of the beam pattern and the spectrum profile, which were then used as the inputs for further simulations. Figure 2(a) illustrates the measured normalized optical spectrum of a flexible OLED at different bias currents I_B [22], which shows the peak wavelengths of 620 nm (Red), 553 nm (Green), 454

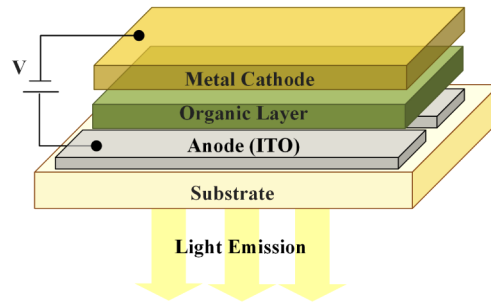


Fig. 1. OLED structure

nm and 480 nm (Blue). The intensity profiles of a flexible OLED for three different configurations are depicted in Fig. 2(b), showing symmetry around 0° but not fitting Lambertian radiation pattern (the solid blue line for $m_L = 1$). Note, the radiation angle $\theta_{1/2}$ ranges are 58° , 65° , 75° , and 90° for the flat, quadrature-circle, half-circle and three quadrature-circle of light panels, respectively. Note that, non-Lambertian emitters can also be considered by Monte Carlo approaches [23]. Instead of a typical Lambertian profile, in the simulation we have used the measured radiation pattern for the curved OLED, which is wider than Lambertian pattern.

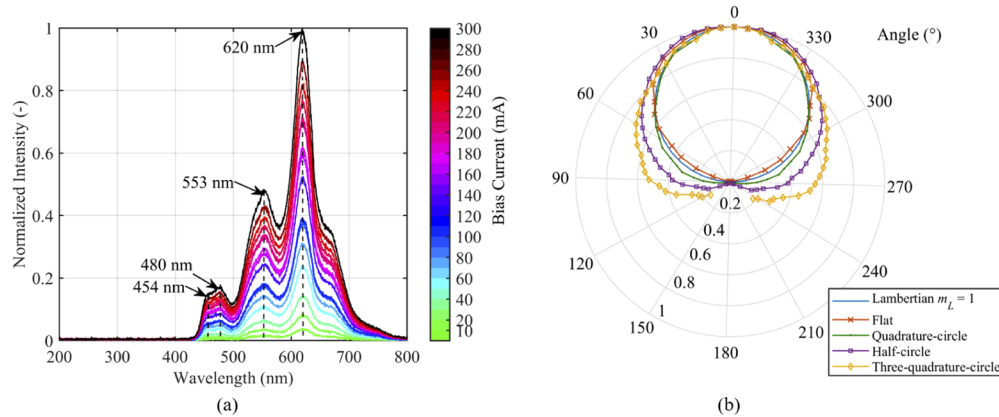


Fig. 2. Characteristics of the flexible OLED adopted in the work: (a) the normalized optical spectrum of the flexible OLED. The peak wavelengths is marked and the legend color scale represents I_B [22]. (b) The intensity pattern of OLED panel bent in different curvature such that we have a quadrature, half and three-quadrature-circle of lighting.

3. Modeling flexible OLED-based VLC within the mall scenario

Figure 3 illustrates the steps adopted in this work for channel modeling. First, an indoor environment or a 3D scene such as office, hospital, store, etc., with specified geometry, shape and with objects is created. This is followed by including the main system parameters for reflection coefficients of different surfaces, and location of light sources and detectors. We have adopted the non-sequential ray tracing feature of Zemax to specify the number of rays, the detected power and the path lengths for each ray. The output data are then imported to Matlab for processing to determine the CIR.

The organic light sources are being widely used in large area including shopping malls, airport, etc, because of flexibility, smooth lighting, etc. Thus the reason why a shopping mall is being

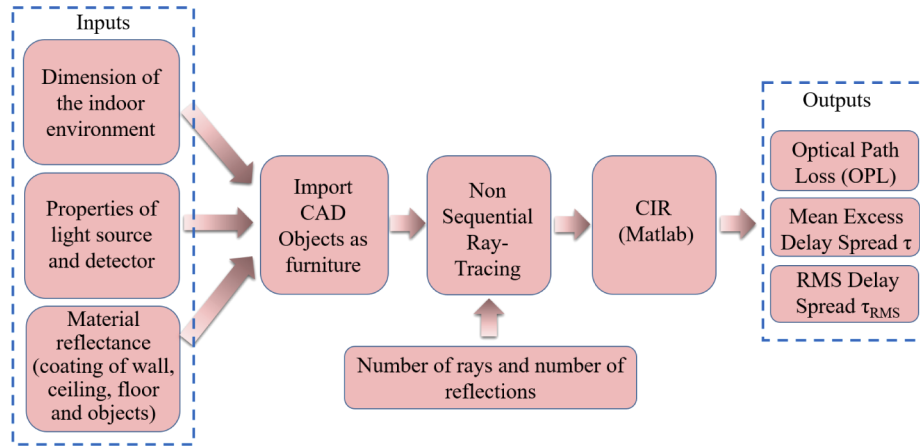


Fig. 3. The major steps followed in the channel modeling methodology.

considered in this work, which can be adopted in other application areas. Figure 4(a) shows a $10 \times 10 \times 3 \text{ m}^3$ size store with a number of objects. Note, the use of curved OLED on the pillar, which is composed of 38 OLED panels 64-chip and with a chip radiating power of 4.1 mW and a total power of 10 W. The size of OLED was set as $2 \times 0.5 \text{ m}^2$. In the model, we adopted measured beam patterns for the curved OLED, see Fig. 5. The reflectance values as a function of the wavelength for a range of surfaces, materials, etc., are shown in Fig. 6, which is adopted from [13,24]. Note that, the specular reflection case is used when materials have specified regular surfaces, which reflect the rays in particular directions and hence the use of Phong model [17,25]. Although specular reflections can occur from shiny objects, in nature (e.g., shopping mall area), where materials have irregular surfaces and rays are reflected in all directions, the resultant reflection pattern is mostly diffuse in nature that can be modeled as Lambertian [13,26,27]. Therefore, the reflections from materials are assumed to be purely diffuse. The Rx is positioned at the height of 1.3 m above the floor level (i.e., the holding position of mobile by people) while the user is facing OLED and its location is varied on the diagonal, which stretches from the corner to the middle of the room. The distance between the Tx and the Rx can be within the range of $0.5 \text{ m} < d_{\text{LOS}} < 6 \text{ m}$. Note, the dimension of the user considered is $25 \times 50 \times 180 \text{ cm}^3$.

We have considered 4 scenarios of (i) a full-circular OLED panel around the pillar in an empty (S_1) and a furnished room (S_2), see Fig. 4(b); and (ii) a half-circular OLED panel (size of $1 \times 0.5 \text{ m}^2$) in an empty room (S_3) and in a furnished room (S_4), see Fig. 4(c). Here, we have adopted Monte Carlo analysis and Sobol sampling as the random ray-tracing methods. The number of reflections was set based on the simulation of particular ray propagation, where the normalized intensity dropped to 10^{-3} . All other key system parameters are given in Table 1.

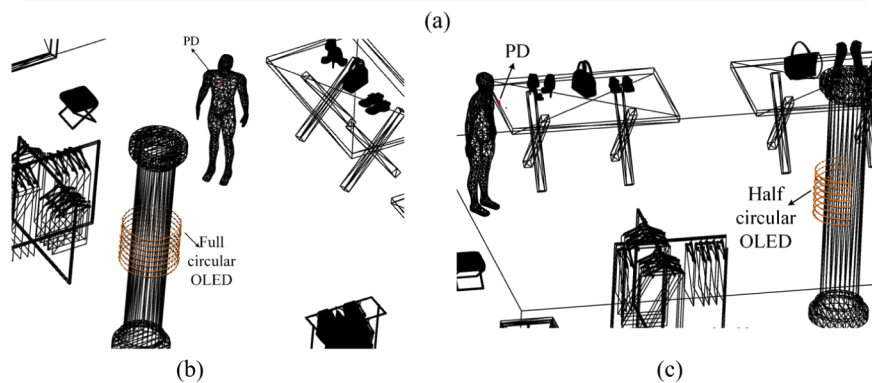
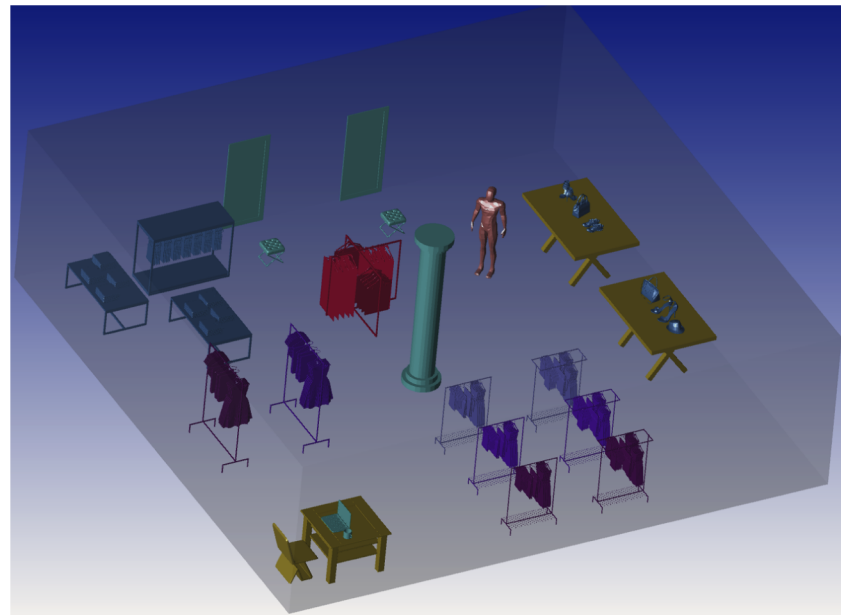


Fig. 4. (a) The three-dimensional indoor environment in Zemax and proposed scenarios; showing the location of curved OLED giving (b) a full-circular lighting and (c) a half-circular lighting.

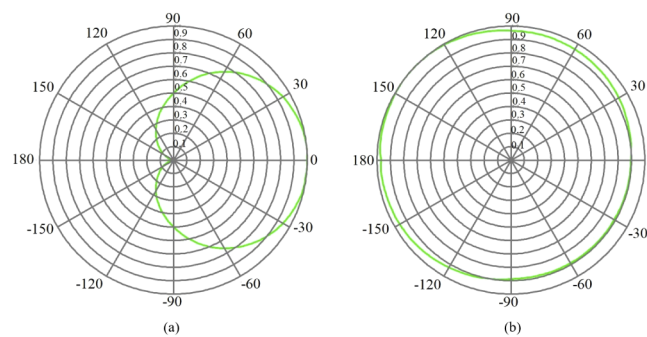


Fig. 5. Emission pattern of the light source used in simulation for: (a) a half-circular OLED and (b) a full-circular OLED.

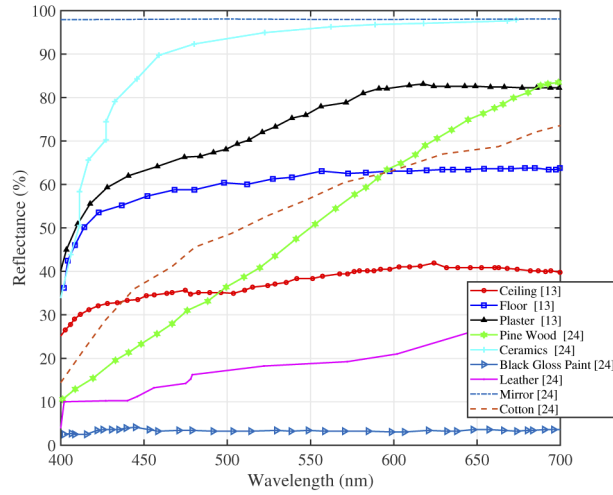


Fig. 6. Spectral reflectance of various materials used in simulation [13,24].

Table 1. System and Simulation Parameters

Item	Parameter	Value
Room	Size	$10 \times 10 \times 3\text{m}^3$
	Radius of pillar	33 cm
Reflections specifications	Type of reflections	Purely diffuse
	Number of reflections	4
	Material reflectance	Wavelength-dependent
Coating material	Walls and pillar	Plaster
	Desks and chair	Pine wood
	Couch, shoes, and bags	Leather
	Laptop	Black gloss paint
	Coffee cup	Ceramics
	Clothes	Cotton
Tx	Dimension	$2 \times 0.5\text{m}^2$
	Type	Flexible OLED
	Bandwidth	50 kHz
	Power of lighting	10 W
	Number of OLED panels	38
	Number of chip per each panel	64
	Power of each chip	4.1 mW
	Location on pillar	Fixed (Middle of store)
Channel	Length d_{LOS}	1 m to 6 m
	Resolution time	0.2 ns
Rx	Active area of PD	1 cm^2
	FOV angle	90°
	Responsivity	0.4 A/W
	N_0	10^{-21} W/Hz

4. Results

The results from analyzes are discussed in this section.

4.1. CIR characteristics

The channel OPL can be used to specify the required emitting power of light source to meet the BER target. At first we make a comparison of inorganic LED and OLED sources with the results shown in Fig. 7. As can be seen, for the LED, OPL is increased by ~ 5 dB compared with S_4 . In addition, τ_{RMS} for S_4 is considerably lower than LED-based VLC. Note, the main purpose, however, was to provide comparison of the utilization of curved OLEDs.

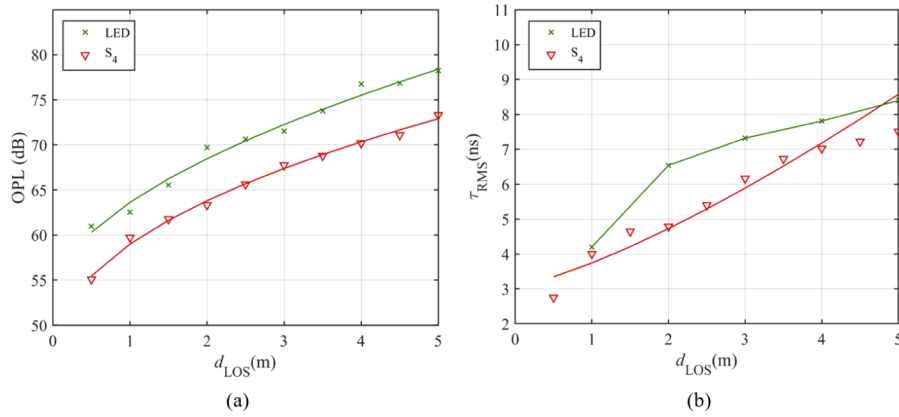


Fig. 7. Comparison of inorganic LED with half-circular OLED (i.e., S_4) in the furnished room in term of: (a) OPL and (b) τ_{RMS} .

Figure 8(a) shows OPL distributions of the curved OLED sources for S_1 and S_2 . The OPL increases with the LOS path reaching maximum values of 69 and 74 dB at d_{LOS} of 6 m for S_1 and S_2 , respectively. For S_2 , OPL is higher compared with S_1 due to the lower reflection coefficients of the objects within the room. It can be seen that, for $d_{\text{LOS}} > 4$ m, there is a huge difference in the received power between the empty and furnished rooms. E.g., the OPL penalties are 2.6, 3.8

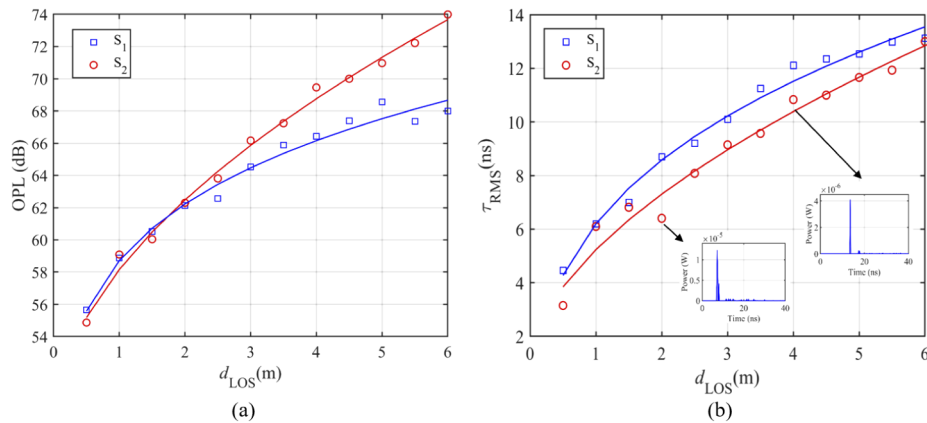


Fig. 8. Comparison of empty and furnished room where a full-circular OLED is employed (i.e., S_1 and S_2) in term of: (a) OPL and (b) τ_{RMS} . The CIR plots for distance of 2 m and 4 m are shown in inset.

and 4.9 dB for d_{LOS} of 4, 5 and 6 m, respectively. As an example, CIR plots for d_{LOS} of 2 and 4 m are shown in insets of Fig. 8(b) depicting τ_{RMS} as a function of d_{LOS} for S_1 and S_2 . Note, τ_{RMS} increases with d_{LOS} reaching maximum values of 13.55 and 12.85 ns at the corner for S_1 and S_2 , respectively.

Figure 9 shows OPL and the delay spread as a function of d_{LOS} for S_3 and S_4 when using a half-circular OLED in empty and furnished rooms, which are higher and lower, respectively, compared with Fig. 8 for a given d_{LOS} . In an empty room, OPL reaches the maximum of 71 dB, which is lower than the value corresponding to S_4 (75 dB). As a result of the comparison between scenarios of S_2 and S_4 OPL decreases at the cost of increasing τ_{RMS} , where a full-circular OLED is employed in a furnished room compared with a half-circular OLED. The OPL penalty improvement is approximately 1.6 dB.

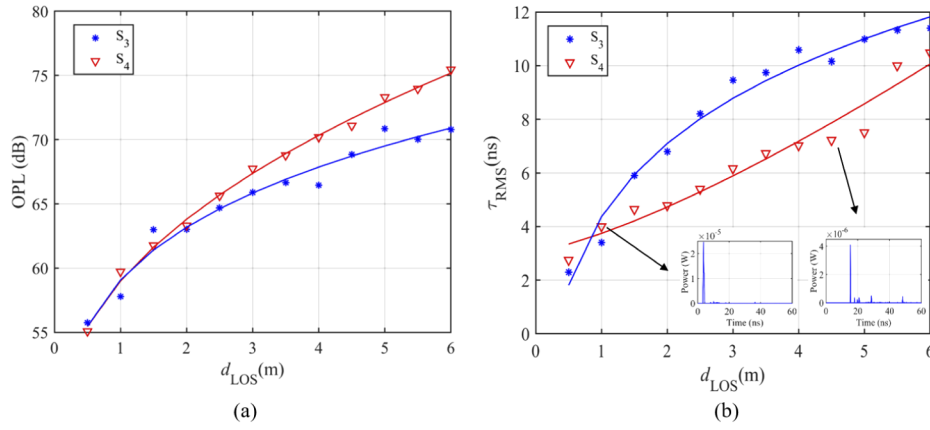


Fig. 9. Comparison of empty and furnished room where a half-circular OLED is employed (i.e., S_3 and S_4) in term of: (a) OPL and (b) τ_{RMS} . The CIR plots for distance of 1 m and 4.5 m are shown in inset.

Based on numerical modeling, we have derived empirical models for d_{LOS} and τ_{RMS} . For all cases the delay spread is obtained by fitting a 2-term power series model, which is given as:

$$\tau_{\text{RMS}} = t_1 d_{\text{LOS}}^2 + t_3, \quad (7)$$

where t_1 , t_2 and t_3 for the scenarios considered here are summarized in Table 2. In addition, for all cases using the 2-term power series models we have:

$$\text{OPL} = o_1 d_{\text{LOS}}^2 + o_3, \quad (8)$$

where the parameters o_1 , o_2 and o_3 are given in Table 3. Note, the main aim of this paper is to investigate the behavior/trends of OPL and τ_{RMS} and show that the empirical parameters, which are valid for the specific room size, can vary based on the number of objects in the room and the room-size.

Table 2. Numerical modeling parameters for τ_{RMS} in all proposed scenarios (S_1 , S_2 , S_3 , S_4).

Scenario	t_1	t_2	t_3
S_1	6.2500	0.4381	1.156×10^{-9}
S_2	5.1972	0.5017	7.462×10^{-9}
S_3	4.5961	0.5481	1.468×10^{-12}
S_4	0.6643	1.3132	3.0756

Table 3. Numerical modeling parameters for OPL in all proposed scenarios (S_1, S_2, S_3, S_4).

Scenario	α_1	α_2	α_3
S_1	29.59	0.1618	29.13
S_2	9.568	0.5378	48.59
S_3	29.07	0.1905	30.00
S_4	13.43	0.4414	45.56

4.2. System performance

The BER performance of the proposed system with non-return-to-zero (NRZ) on-off keying (OOK) is shown in Fig. 10. Also shown is the 7% forward error correction (FEC) BER limit of 3.8×10^{-3} . For S_1 , the BER plots are below the FEC limit for d_{LOS} up to 6 m with R_b of 10 Mb/s. For S_2 , BER values lower than the FEC are achieved at d_{LOS} of < 4 m with R_b of up to 10 Mb/s. In addition, R_b values are 3.04 and 1.02 Mb/s for d_{LOS} of 5 and 6 m, respectively for S_2 . Figure 10(b) depicts the BER for S_3 and S_4 , where S_3 shows improved performance over a longer distance compared with S_4 . It can be seen that, for S_3 the BER remains just below the FEC limit for $d_{LOS} < 4$ m and at d_{LOS} of 5 and 6 m the achieved R_b values are 7.05 and 3.7 Mb/s, respectively. For S_4 , the BER is also below the FEC limit for d_{LOS} of < 3 m with R_b of 10 Mb/s. Additionally, R_b values are 4.82, 1.48 and 0.46 Mb/s for d_{LOS} of 4, 5 and 6 m, respectively.

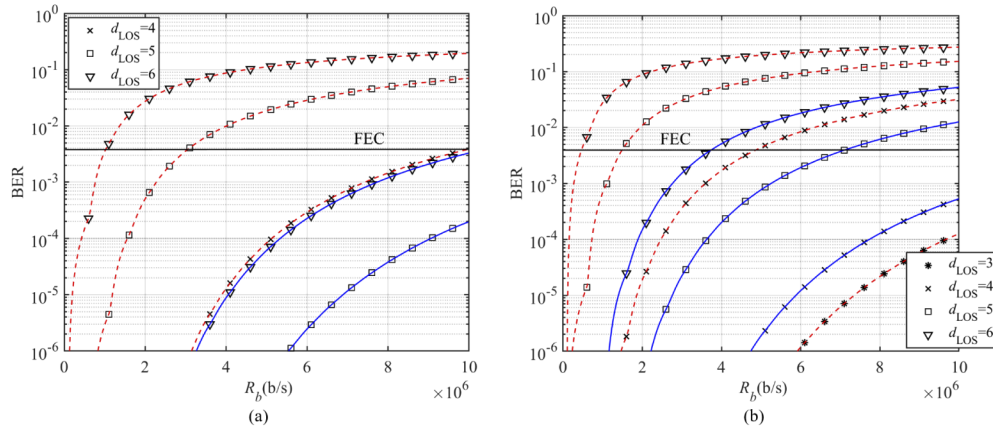


Fig. 10. The BER performance versus R_b for different d_{LOS} in cases of: (a) S_1 (solid blue line), S_2 (dashed red line) and (b) S_3 (solid blue line), S_4 (dashed red line).

Figure 11 illustrates the channel capacity C versus the transmit optical power P_E for a range of d_{LOS} at R_b of 4 Mb/s and B_{mod} of 50 kHz for S_1 - S_4 . It can be seen that, C increases with respect to P_E . E.g., for S_2 , at d_{LOS} of 3 m we observe C of 4.46 and 17.83 Mb/s at P_E of 10 and 20 W, respectively. Obviously, for the same P_E a significant drop in C can be seen with increased d_{LOS} ; e.g., for S_1 , at P_E of 10 W, C drops from 23.78 to 1.23 Mb/s for d_{LOS} of 2 and 6 m, respectively. For S_1 , it is observed that for $d_{LOS} < 3$ m and $P_E > 20$ W, C is higher than 100 Mb/s. For S_3 and S_4 , we observe the same trend for C as in Fig. 11(a), see Fig. 11(b). It can be seen that, for the same d_{LOS} , almost similar channel capacity can be achieved with lower emitted optical power in the case of S_2 compared with S_4 as the light source dimension increases. E.g., at d_{LOS} of 3 m, C of 10 Mb/s can be achieved for power levels of 15 and 22 W for S_2 and S_4 , respectively. As a result of the comparison between all scenarios; e.g., at a given P_E of 20 W and d_{LOS} of 4 m, we have C of 15.58, 4.71, 7.11 and 2.28 Mb/s for S_1 to S_4 , respectively. Therefore, there is a

significant drop in C for the case of furnished room compared with an empty room, regardless of using a full or a half-circular OLED.

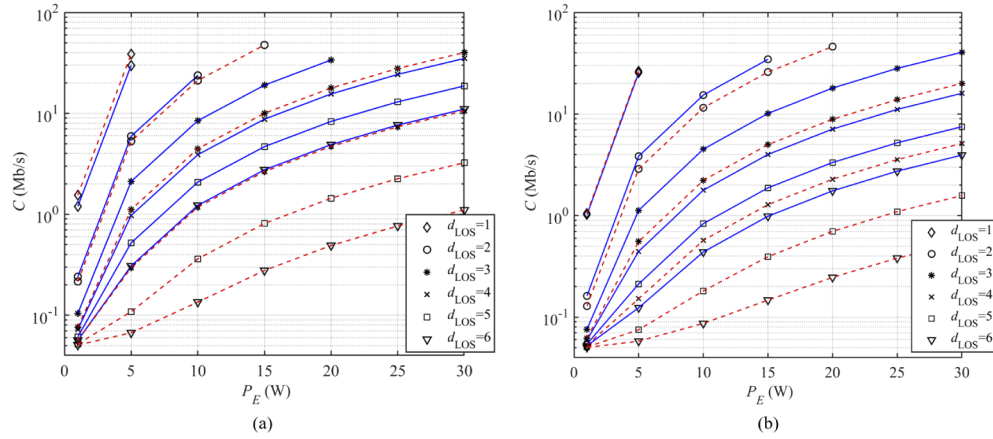


Fig. 11. The channel capacity versus P_E for different d_{LOS} at R_b of 4 Mb/s and B_{mod} of 50 kHz for: (a) S_1 (solid blue line), S_2 (dashed red line) and (b) S_3 (solid blue line), S_4 (dashed red line).

5. Conclusion

In this paper, we proposed a flexible OLED as the Tx in a VLC system to cover the shopping mall. We carried out the characterization of the OLED in terms of the spectrum profile and optical irradiation pattern as part of the simulation modeling of the light source. The beam pattern of a curved OLED was found to be symmetrical about the origin while being wider than Lambertian radiation pattern. This feature offers the benefit of maintaining the same SNR over a given transmission radius of curved OLED. The increasing use of flexible OLED in thin-film devices (such as wearable devices, mobile phones, TVs) acts as a good motivator to investigate the performance of a VLC system based on these devices. The results of utilizing a full-circular OLED for both empty and furnished rooms showed a uniform distribution of emitted power for the same transmission link spans. We showed that for full and half-circular OLEDs adopted in an empty room, the link performance improved with the average OPL penalties of 5 and 4 dB compare with the corner of a furnished room. The numerical models of τ_{RMS} were derived, which followed a 2-term power series model for both the empty and furnished rooms. In addition, the OPL profile models were derived for all proposed scenarios. Furthermore, the link's BER performance and the channel capacity were investigated. For an empty room with full and half-circular OLEDs, R_b of 10 and 3.7 Mb/s were achieved at d_{LOS} of 6 m, respectively. In addition, in a furnished room with a full-circular OLED, R_b of 10, 3.04 and 1.02 Mb/s were recorded for d_{LOS} of 4, 5 and 6 m, respectively, which are two times higher than the values when using a half-circular OLED (i.e., 4.82, 1.48 and 0.46 Mb/s). As a result, for a given d_{LOS} the same channel capacity can be obtained with lower emitted optical power using a full-circular light source compared with a half-circular OLED.

Funding

H2020 Marie Skłodowska-Curie Actions (VisIoN 764461).

Disclosures

The authors declare no conflicts of interest.

References

1. Z. Ghassemlooy, L. N. Alves, S. Zvanovec, and M.-A. Khalighi, *Visible light communications: theory and applications* (CRC press, 2017).
2. Z. Ghassemlooy, W. Popoola, and S. Rajbhandari, *Optical wireless communications: system and channel modelling with Matlab®* (CRC press, 2019).
3. B. Lin, Z. Ghassemlooy, C. Lin, X. Tang, Y. Li, and S. Zhang, "An indoor visible light positioning system based on optical camera communications," *IEEE Photonics Technol. Lett.* **29**(7), 579–582 (2017).
4. S. Schmid, T. Richner, S. Mangold, and T. R. Gross, "Enlighting: An indoor visible light communication system based on networked light bulbs," in *2016 13th Annual IEEE International Conference on Sensing, Communication, and Networking (SECON)*, (IEEE, 2016), pp. 1–9.
5. B. Geffroy, P. Le Roy, and C. Prat, "Organic light-emitting diode (oled) technology: materials, devices and display technologies," *Polym. Int.* **55**(6), 572–582 (2006).
6. J. Clark and G. Lanzani, "Organic photonics for communications," *Nat. Photonics* **4**(7), 438–446 (2010).
7. J. Ràfols-Ribé, P.-A. Will, C. Hänisch, M. Gonzalez-Silveira, S. Lenk, J. Rodríguez-Viejo, and S. Reineke, "High-performance organic light-emitting diodes comprising ultrastable glass layers," *Sci. Adv.* **4**(5), eaar8332 (2018).
8. Z. H. Kafafi, *Organic electroluminescence* (CRC Press, 2018).
9. H. Chun, C.-J. Chiang, and D. C. O'Brien, "Visible light communication using oleds: Illumination and channel modeling," in *2012 International Workshop on Optical Wireless Communications (IWOW)*, (IEEE, 2012), pp. 1–3.
10. H. Nguyen, J.-H. Choi, M. Kang, Z. Ghassemlooy, D. Kim, S.-K. Lim, T.-G. Kang, and C. G. Lee, "A matlab-based simulation program for indoor visible light communication system," in *2010 7th International Symposium on Communication Systems, Networks & Digital Signal Processing (CSNDSP 2010)*, (IEEE, 2010), pp. 537–541.
11. T. Komine and M. Nakagawa, "Performance evaluation of visible-light wireless communication system using white led lightings," in *Proceedings. ISCC 2004. Ninth International Symposium on Computers And Communications (IEEE Cat. No. 04TH8769)*, vol. 1 (IEEE, 2004), pp. 258–263.
12. J. R. Barry, J. M. Kahn, W. J. Krause, E. A. Lee, and D. G. Messerschmitt, "Simulation of multipath impulse response for indoor wireless optical channels," *IEEE J. Select. Areas Commun.* **11**(3), 367–379 (1993).
13. K. Lee, H. Park, and J. R. Barry, "Indoor channel characteristics for visible light communications," *IEEE Commun. Lett.* **15**(2), 217–219 (2011).
14. F. Miramirkhani and M. Uysal, "Channel modeling and characterization for visible light communications," *IEEE Photonics J.* **7**(6), 1–16 (2015).
15. Zemax OpticStudio 18.9, <https://www.zemax.com/products/opticstudio>.
16. M. Uysal, F. Miramirkhani, O. Narmanlioglu, T. Baykas, and E. Panayirci, "Ieee 802.15. 7r1 reference channel models for visible light communications," *IEEE Commun. Mag.* **55**(1), 212–217 (2017).
17. S. P. Rodríguez, R. P. Jiménez, B. R. Mendoza, F. J. L. Hernández, and A. J. A. Alfonso, "Simulation of impulse response for indoor visible light communications using 3d cad models," *J Wireless Com Network* **2013**(1), 7 (2013).
18. H. Chen and Z. Xu, "Oled panel radiation pattern and its impact on vlc channel characteristics," *IEEE Photonics J.* **10**(2), 1–10 (2018).
19. S. Long, M.-A. Khalighi, M. Wolf, Z. Ghassemlooy, and S. Bourennane, "Performance of carrier-less amplitude and phase modulation with frequency domain equalization for indoor visible light communications," in *2015 4th International Workshop on Optical Wireless Communications (IWOW)*, (IEEE, 2015), pp. 16–20.
20. Z. Wang, Q. Wang, W. Huang, and Z. Xu, *Visible light communications: Modulation and signal processing* (John Wiley & Sons, 2017).
21. J. Kalinowski, *Organic Light-Emitting Diodes: Principles, Characteristics & Processes* (CRC press, 2018).
22. Z. N. Chaleshtori, A. Burton, Z. Ghassemlooy, and S. Zvanovec, "A flexible oled based vlc link with m-cap modulation," in *2019 15th International Conference on Telecommunications (ConTEL)*, (IEEE, 2019), pp. 1–6.
23. H. B. Eldeeb, F. Miramirkhani, and M. Uysal, "A path loss model for vehicle-to-vehicle visible light communications," in *2019 15th International Conference on Telecommunications (ConTEL)*, (IEEE, 2019), pp. 1–5.
24. ASTER Spectral Library-Version 2.0, <http://speclib.jpl.nasa.gov>.
25. S. Lee, J. K. Kwon, S.-Y. Jung, and Y.-H. Kwon, "Evaluation of visible light communication channel delay profiles for automotive applications," *J Wireless Com Network* **2012**(1), 370 (2012).
26. C. R. Lomba, R. T. Valadas, and A. de Oliveira Duarte, "Efficient simulation of the impulse response of the indoor wireless optical channel," *Int. J. Commun. Syst.* **13**(7-8), 537–549 (2000).
27. C. R. Lomba, R. T. Valadas, and A. de Oliveira Duarte, "Experimental characterisation and modelling of the reflection of infrared signals on indoor surfaces," *IEE Proc.: Optoelectron.* **145**(3), 191–197 (1998).